

01 Feb 2004

Optical Characterization of Ceramic Thin Films: Applications in Low-temperature Solid Oxide Fuel-Cell Materials Research

Vladimir Petrovsky

Tatiana Petrovsky

Harlan U. Anderson

Missouri University of Science and Technology, harlanua@mst.edu

Brian P. Gorman

Follow this and additional works at: https://scholarsmine.mst.edu/matsci_eng_facwork

 Part of the [Materials Science and Engineering Commons](#)

Recommended Citation

V. Petrovsky et al., "Optical Characterization of Ceramic Thin Films: Applications in Low-temperature Solid Oxide Fuel-Cell Materials Research," *Journal of Materials Research*, Materials Research Society, Feb 2004. The definitive version is available at <https://doi.org/10.1557/JMR.2004.0070>

This Article - Journal is brought to you for free and open access by Scholars' Mine. It has been accepted for inclusion in Materials Science and Engineering Faculty Research & Creative Works by an authorized administrator of Scholars' Mine. This work is protected by U. S. Copyright Law. Unauthorized use including reproduction for redistribution requires the permission of the copyright holder. For more information, please contact scholarsmine@mst.edu.

Optical characterization of ceramic thin films: Applications in low-temperature solid oxide fuel-cell materials research

B.P. Gorman,^{a)} V. Petrovsky, H.U. Anderson, and T. Petrovsky

Electronic Materials Applied Research Center, University of Missouri–Rolla, Rolla, Missouri, 65409

(Received 28 July 2003; accepted 28 October 2003)

Characterization of thin film solid oxide fuel-cell materials can be difficult due to the range of porosities in electrodes and electrolytes as well as the nano-sized pores and particles. In this study, optical characterization techniques such as ultraviolet–visible transmission and reflection spectrophotometry are illustrated as methods for achieving information about the film density from the film refractive index as well as the film thickness. These techniques were used to investigate the sintering process of colloidal CeO₂ on sapphire substrates and polymeric precursor-derived ZrO₂:16%Y (YSZ) thin films on silicon over the temperature range 400–1000 °C, and the results were compared with traditional characterization techniques such as electron microscopy, profilometry, ellipsometry, and x-ray diffraction line broadening analyses. Most of the techniques were in good agreement with the CeO₂ grain size changing from 5–65 nm and the film thickness changing from 0.8–0.5 μm. Comparisons of transmission and reflection spectrophotometry with ellipsometry illustrated that scattering effects from the porous CeO₂ films caused an overestimation of the refractive index from ellipsometry, but allowed for accurate grain size measurements from transmission and reflection data. Both techniques were in good agreement during the sintering of the YSZ thin films, with the density changing from 90–100% theoretical after heating between 400 and 800 °C.

I. INTRODUCTION

Thin film inorganic solid oxide fuel-cell (SOFC) structures have seen a large increase in research because of the possibility for decreased operating temperatures and concomitant increase in reliability and performance. To maintain microstructural integrity and retain full density, thin film electrolytes should have nanocrystalline grain sizes to prevent pinhole defects.¹ These grain sizes may have effects on the electrical and optical properties as well as the morphology of the resulting surface.^{2,3}

Thin film electrodes with nano-sized porosity are being developed to prevent microstructural defects in the electrolyte. In most thin film electrolyte SOFC structures, the porous electrode also acts as the support for the electrolyte. If the surface roughness resulting from large pores in the electrode is similar to the thickness of the electrolyte, electrical shorts or holes in the electrolyte may result, decreasing the efficiency of the device. Graded porosity electrodes are currently being developed where a thin electrode film with nano-sized porosity is

deposited on macroporous substrates to process electrolytes with thickness less than 1 μm.⁴

Decreasing the feature sizes to these small dimensions (typically less than 10 nm) also increases the difficulty of microstructural characterization. X-ray diffraction (XRD) line broadening has been used to estimate grain sizes in the nanocrystalline (<100 nm) regime using Williamson–Hall or Warren–Averbach analyses.^{5,6} These techniques can be highly effective in estimating the film grain size, but care must be taken to separate line-broadening contributions from both grain size and strain effects in thin film structures. Profilometry and electron microscopy (scanning electron microscopy and transmission electron microscopy) can give accurate information about microstructural features such as grain size and film thickness, with a resolution to approximately 5 nm.⁷ In addition, high-resolution transmission electron microscopy (HRTEM) has been shown to give accurate spatial dimensions of 2 Å or less.⁸ Unfortunately, none of these microstructural characterization techniques give quantitative information about the film density, especially with pore sizes in the nanometer range.

In bulk structures, density and pore size are measured using either mercury porosimetry⁹ or nitrogen adsorption.¹⁰ In thin film structures, however, the small volume

^{a)}Present address: Department of Physics, University of North Texas, Denton, TX 76203.

of sample does not allow for accurate measurements using these techniques. Actual film density can also be measured using surface acoustic wave spectroscopy, but the density is inherently tied to the elastic modulus, and the separation may cause errors.¹¹ Optical characterization techniques such as ellipsometry and ultraviolet–visible (UV–V) spectrophotometry have been shown to give information about the density.^{12,13} This is determined from the high-frequency film refractive index via mixing rules such as Lorentz–Lorenz or effective medium theory. Unfortunately, these techniques do not give pore-size distributions or the nature of the porosity (open or closed).

Measurements of thin film thickness can also be accomplished using ellipsometry and UV–V spectrophotometry. In both techniques, the film thickness and refractive index are inherently calculated together by modeling the structures. In addition, UV–V techniques also allow for the measurement of the grain size in porous thin films by factoring out the scattering intensity from the extinction coefficient.¹²

CeO₂ was chosen as a representative material for this study due to its potential applications as thin films in solid oxide fuel-cell electrolytes and electrodes.^{14–16} Thin films of pure CeO₂ were processed using a colloidal deposition technique and its sintering characteristics measured using all of the techniques mentioned above. ZrO₂:16% Y (Yttrium-stabilized zirconia) films (typically used as dense electrolytes), processed using a polymeric precursor spin coating technique, were investigated according to their density changes using ellipsometry and UV–V spectrophotometry.

II. EXPERIMENTAL

Processing of nanoporous CeO₂ thin films has been outlined in detail elsewhere⁷ and will briefly be summarized here. Nanocrystalline CeO₂ powder (initial grain size approximately 5 nm) was produced using an aqueous precipitation processing route. Cerium (III) nitrate (99.999%, Alfa Aesar, Inc., Ward Hill, MA) was dissolved in distilled water and precipitated using hydrogen peroxide and ammonium hydroxide, similar to the technique in Ref. 17. The hydrated powder was then annealed at 150 °C to form the full fluorite structured material. Aqueous colloidal suspensions were prepared by mixing 10 wt.% of the nanocrystalline CeO₂ in pH 5 distilled water (balanced with HNO₃) along with 5 wt.% butoxy-ethanol to aid in drying and to improve the wetting characteristics. The mixture was then dispersed using a high-intensity ultrasonic probe for about 1 h. After the powder was well dispersed, the solution was filtered through a 0.45- μ m glass fiber filter (Whatman, Inc., Clifton, NJ) and spin-coated on optical quality (0001) sapphire substrates. The films were subsequently dried at 350 °C,

followed by sintering at their respective temperatures (400, 600, 700, 800, 900, and 1000 °C) for 2 h.

YSZ polymeric precursors were prepared using a technique outlined in Ref. 8. Reagent-grade cation salts [ZrOCl₂ and Y(NO₃)₃] were dissolved in water, added to a solution of ethylene glycol, tartaric acid, and nitric acid, and placed on a stirring hot plate at 70 °C for 40 h. The resulting precipitate-free precursor was spin-coated on sapphire substrates, dried at 70 °C for 1 h, and pyrolyzed at 350 °C for 10 min. Films were subsequently annealed in a standard furnace for 2 h using an air atmosphere.

Profilometry (Sloan Dektak II, Veeco Instruments, Woodbury, NY) was used to determine the CeO₂ film thickness after each annealing temperature. Each of the respective samples were scored using a diamond-tipped scribe and scanned perpendicular to the scribe at low speed. The film thickness could be determined from the resulting height. It was determined, using five scribes on a single sample, that the variance associated with the thickness measurement was ± 70 nm. X-ray diffraction (XDS 2000 Scintag, Cupertino, CA) was also used to determine the CeO₂ crystal structure. Texturing of the films as well as any reactions with the sapphire substrates after sintering at each temperature was not observed.¹² Williamson–Hall line broadening analyses were utilized to determine the CeO₂ grain size and film strain. Analyses indicated that strains in these films were minimal. Repeatability of the grain size calculations were of the order 1 nm, which is similar to that seen in other studies.⁶

Field-emission scanning electron microscopy (FE-SEM, Hitachi S4700, Pleasanton, CA) was utilized in this investigation to determine the CeO₂ film grain size and thickness. Annealed film surfaces and fracture cross-sections were mounted using double-sided carbon tape and coated using evaporated carbon. Images were acquired using an accelerating voltage of 5 kV and a working distance of 7 mm. Grain sizes and film thickness were determined by digitally measuring the features on the images using NIH image (National Institute of Health Research Services Branch, Bethesda, MD) analysis software. Each of these features were measured by acquiring the number of pixels in the feature length (P_f) and dividing by a standardization factor. The standardization factor is equal to the number of pixels in a known length (P_s) divided by the known length (L_s). To determine the errors associated with the measurement of the film thickness, grain size, and refractive index, a standard error analysis was performed. The total error associated with each measurement can be described by:¹⁸

$$\delta^2 = \sum_i \left(\frac{\partial K}{\partial \chi_i} \right)^2 \cdot \sigma_{\chi_i}^2, \quad (1)$$

where δ is the error associated with the measurement, K is the quantity measured, χ_i is the individual variable, and σ_{χ_i} is the variance of each variable.

Null ellipsometry (Gaertner Scientific, Skokie, IL) was used in this investigation to determine the film thickness and refractive index at 633 nm. Measurements were taken at different incident angles from the as-sintered surfaces to ensure good ellipsometric order. According to the manufacturer, errors associated with these measurements are 1 Å for the thickness and 0.001 for the refractive index, again assuming good ellipsometric order.

UV–V spectrophotometry (Cary 5, UV-V-NIR Varian Inc., Palo Alto, CA) was utilized in this investigation in both reflectance and transmittance mode to determine the film thickness, refractive index, absorption and bandgap, as well as the scattering coefficients over the wavelength region 300 to 700 nm. Transmittance spectra were normalized using the spectra generated from the beam with no sample and with a sapphire substrate alone. Reflectance spectra were normalized using a spectrum acquired from an uncoated, clean sapphire substrate.

Standard Fresnel equations were used for the calculation of the film refractive index and thickness. Using the summation method outlined previously,^{12,19,20} the film refractive index and thickness could be calculated from the reflection spectra or the transmittance spectra if the extinction coefficient was small compared to the real part of the refractive index. Assuming the substrate is thick enough to eliminate interference, the reflectance and transmittance intensity can be approximated via:

$$R = r^*r + t^*t \cdot r^*r \cdot t^*t' \quad (2)$$

$$T = t^*t \cdot t'^*t' \quad ,$$

where r is the reflectance of the air–film or film–substrate boundaries, and t and t' are the transmittances of the boundaries by the inner and outer surfaces of the substrate. To account for the extinction part of the refractive index, the complex conjugates (r^* and t^*) were used in these equations.

Porosity in the CeO₂ films were determined from the measured refractive index via the Lorentz–Lorenz equation

$$\frac{n'^2 - 1}{n'^2 + 2} = \frac{n^2 - 1}{n^2 + 2} (1 - P) \quad . \quad (3)$$

where n' is the real portion of the measured refractive index from either the spectrophotometric or ellipsometric measurements, n is the theoretical refractive index of fully dense CeO₂ or YSZ, and P is the fraction of porosity in the film.

From the sum of the reflection and transmission spectra, the film extinction coefficient could be calculated. This imaginary part of the refractive index originates from the combination of scattering and absorption, which can be separated mathematically. Rayleigh statistics gives the dependence of the scattering on the defect (grain) size¹²

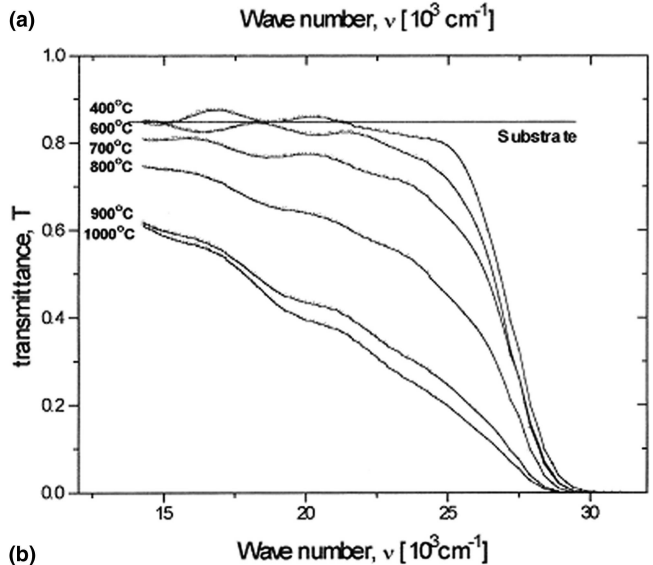
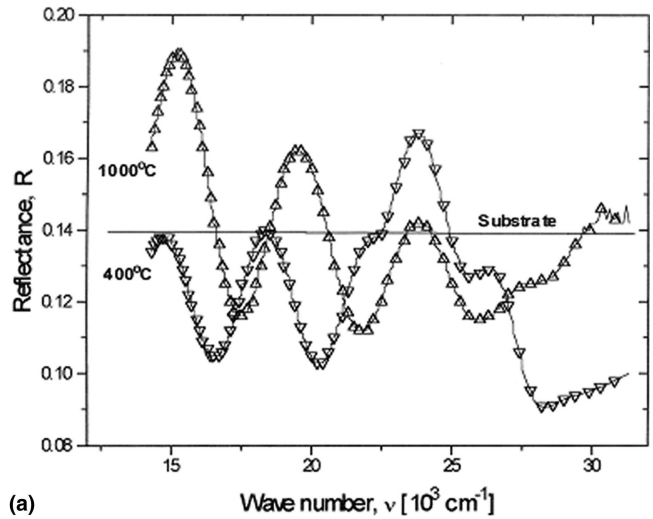


FIG. 1. UV–V spectrophotometry plots of CeO₂ thin films deposited on sapphire substrates and annealed at different temperatures: (a) transmittance and (b) reflectance spectra.

$$k_{\text{scat}} = AP(n) \left(\frac{d}{\lambda} \right)^x \quad , \quad (4)$$

where A is a numerical constant ($A = 20$ for this investigation), λ is the photon wavelength, d is the grain size, n is the theoretical refractive index for CeO₂, P is the porosity, and x is a constant ranging from 1 to 3, depending on the pore distribution. A plot of extinction coefficient versus wavelength should have a linear dependence, and x may then be determined. Ultimately, the absorption coefficient can be determined by subtracting the scattering coefficient from the extinction coefficient.

III. RESULTS

Figure 1 shows the raw UV–V spectrophotometry results from both the reflection and transmission geom-

etries.¹² Changes in the interference patterns evident in both the reflection and transmission spectra are due to changes in the refractive index and the film thickness. Changes in the intensity of the transmission spectra in the low absorption region (less than 450 nm) are due to an increase in the scattering intensity. At higher energies, band-to-band electron transitions result in a large amount of absorption.

Representative FE SEM images of the porous CeO_2 films are illustrated in Fig. 2 (as-annealed surfaces) and Fig. 3 (fracture cross-sections). As can be seen, a significant change in both grain size and the film thickness are observed with anneals at 350 and 800 °C. The change in grain size for the CeO_2 films measured by FE-SEM and XRD as well as those predicted from the scattering coefficient of UV-V spectra are shown in Fig. 4. As can be seen, all three techniques give results that are in fairly good agreement over the entire temperature range, with the grain size changing from approximately 5–65 nm.

Error analysis of the FE SEM feature size measurement technique can yield different results, depending on the resolution of the image (size of P_f and P_s) as well as the ratio of P_f to P_s . As seen in Table I, the calculated percentage error decreases significantly with an increase in resolution, up to 600 dpi. The percentage error also decreases as the ratio of P_f to P_s goes to unity. Thus, to achieve the most accurate measurements from digital microscopy images, the feature sizes should be as close to the length of the standard as is reasonable, and the images should be acquired with the highest resolution possible. In the case of the images used in this investigation, the errors were typically 1.5%.

A significant change in CeO_2 film thickness also occurs after sintering the films, as shown in Fig. 5. Variances in the refractive index and thickness calculations

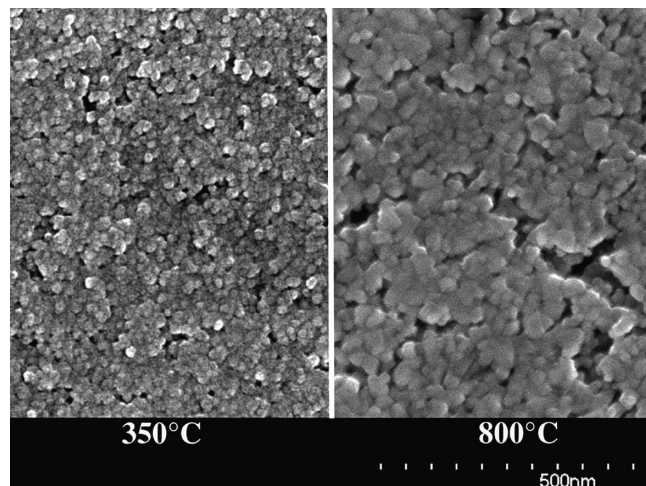


FIG. 2. Surface field-emission scanning electron micrographs of porous CeO_2 films annealed at 350 and 800 °C.

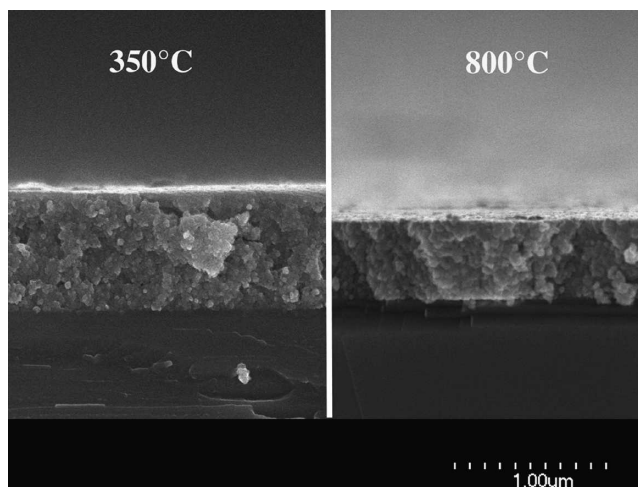


FIG. 3. Cross-sectional field-emission scanning electron micrographs of porous CeO_2 films annealed at 350 and 800 °C.

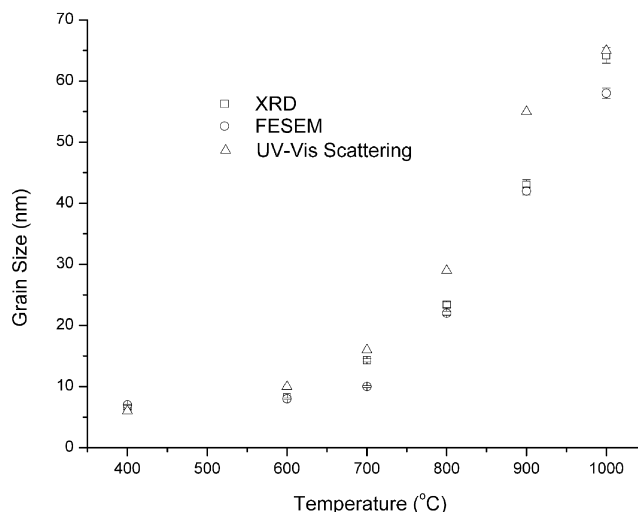


FIG. 4. Change in grain size of the CeO_2 thin films with annealing temperature as measured by different techniques.

TABLE I. Errors associated with feature size measurements from digital micrographs. P_f/P_s is the ratio of measured pixels to the number of pixels in a standard known length

P_f/P_s	5	1	0.5	0.1	0.01
Resolution = 72 dpi	3.7	5.0	7.8	35	350
Resolution = 150 dpi	2.0	2.6	3.9	17	170
Resolution = 300 dpi	1.7	2.2	3.3	14	140
Resolution = 600 dpi	1.3	1.6	2.1	8.4	83
Resolution = 1200 dpi	1.2	1.3	1.6	5.7	56

from UV-V transmission and reflection measurements were found to be approximately 2%. As can be seen, film thickness obtained from UV-V and ellipsometry give similar results. SEM consistently underestimates the film thickness compared with the optical techniques, which may be due to incorrect standardization of L_s or incorrect

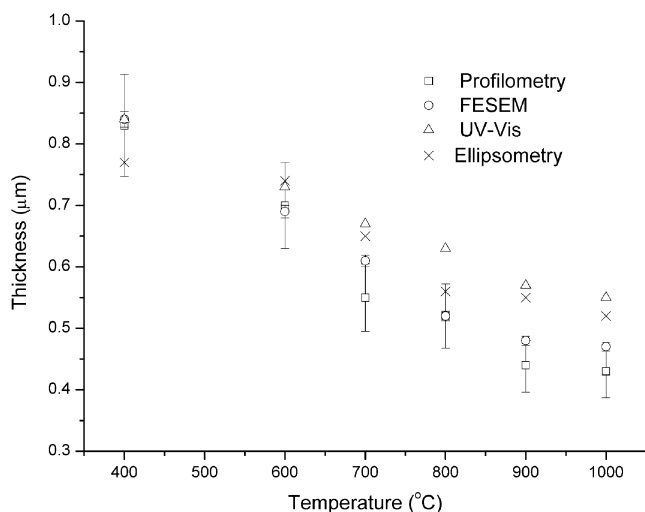


FIG. 5. Change in CeO₂ thin film thickness with annealing temperature as measured by different techniques.

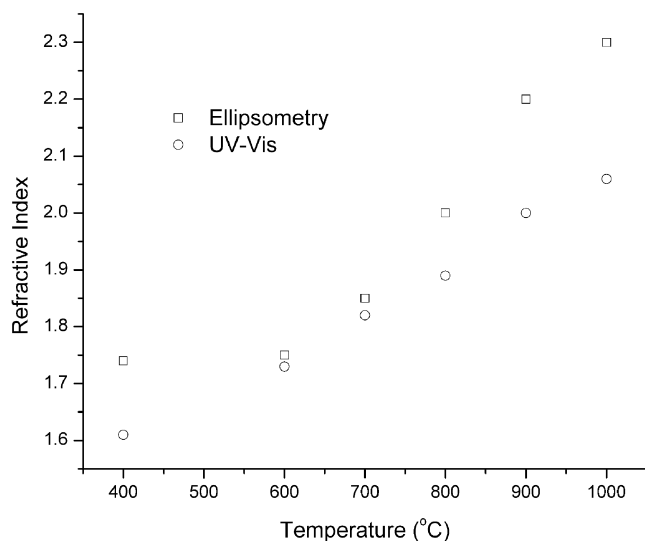


FIG. 6. Change in refractive index with annealing temperature as measured by ellipsometry and UV-V interference spectrophotometry.

definitions of the film-substrate interface. Profilometry also consistently underestimates the film thickness, which most likely is due to inaccuracies in the scribe depth being exactly at the film-substrate interface or from the profile scan rate being too high, resulting in incomplete penetration of the profilometer tip to the bottom of the scribe.

Figure 6 shows the changes in refractive index with the change in annealing temperature for the CeO₂ films as measured by UV-V spectrophotometry and ellipsometry. Both techniques give changes in refractive index between approximately 1.6 and 2.2. Variations in data between these two techniques arise from scattering not being taken into account in the ellipsometry analyses. Spectroscopic ellipsometry can incorporate this scattering

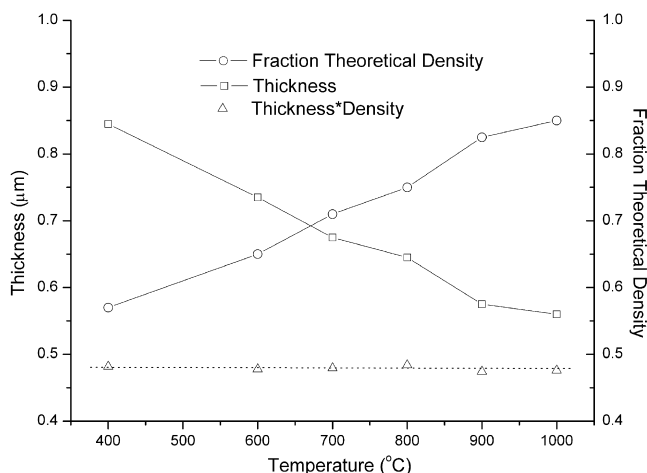


FIG. 7. Change in CeO₂ thin film density as measured by UV-V interference spectrophotometry. Also shown is the thickness-density product, illustrating the validity of the interference technique.

factor and thus should be used in future characterization of porous thin films.

Using Eq. (3), the CeO₂ film density was calculated from the UV-V determined refractive index and is depicted in Fig. 7. As can be seen, the film density changes from 57% initially to 85% after annealing at 1000 °C for 2 h. Also depicted in Fig. 7 is the film thickness multiplied by the film density. This number should be a constant and equal to the volume of material in the film, given the films were coated similarly, resulting in a consistent thickness. As can be seen, this product is a constant over the entire range of grain sizes, film thickness, and densities investigated. Thus, it can be concluded that the errors in the refractive index measurements were indeed due to ellipsometry errors, again most likely due to scattering effects.

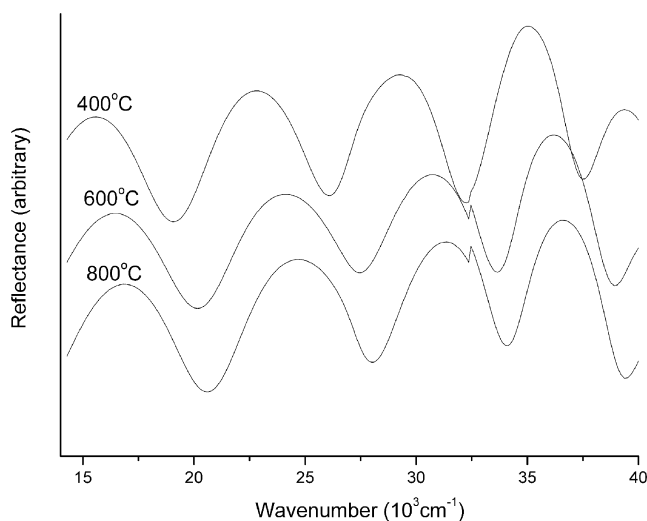


FIG. 8. UV-V spectrophotometry reflection data for YSZ thin films deposited on sapphire substrates and annealed at different temperatures.

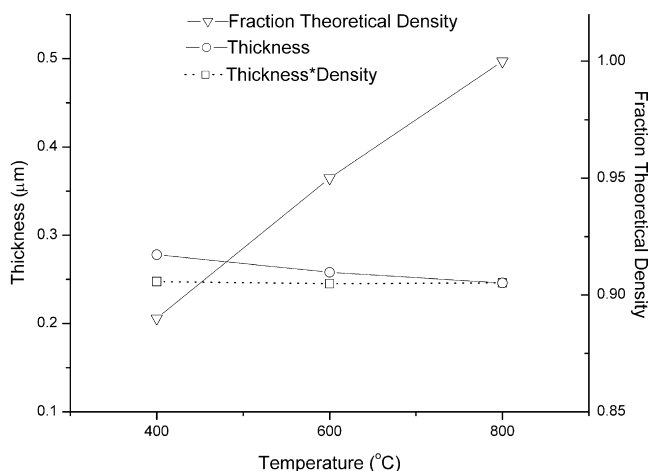


FIG. 9. Change in YSZ film thickness and density as measured by UV–V interference spectrophotometry. Also shown is the thickness–density product, illustrating the validity of the interference technique.

The UV–V reflection data for the YSZ films processed on sapphire substrates and annealed at different temperatures are shown in Fig. 8. The spectra are offset for clarity, but their relative intensities have not been changed. A slight bump visible at $32,000\text{ cm}^{-1}$ is due to a change in the spectrometer grating. It was removed following normalization and thus is not sample-oriented. Fitting this interference data resulted in the thickness and refractive index data shown in Fig. 9. After annealing at 400 °C , the film has a density 90% of theoretical, as opposed to the colloidal-processed CeO_2 films with an initial density of 57%. After annealing at 800 °C , the film achieves full density. Due to its high density and large band gap, there is no scattering or absorption observed in these reflection spectra. The thickness–density product illustrates the accuracy of this technique to not only the porous electrode materials, but also the near full density electrolytes. YSZ processed using the polymeric precursor technique would thus be useful as a SOFC electrolyte due to its density near theoretical at processing temperatures greater than 400 °C .

IV. CONCLUSIONS

Wavelength-dependent interference patterns in the UV–V spectrophotometric measurements can provide quantitative information about thickness and refractive index (and therefore density) of thin film SOFC materials. Optical techniques are applicable to a range of densities where other techniques are not quantitative. The

wavelength dependence of scattering from the UV–V spectrophotometry measurements can also provide quantitative information about grain sizes in a porous thin film, so long as the extinction coefficient is properly removed from the refractive index data. Comparisons of the film grain sizes and thickness obtained by this method correlates well to other already established techniques.

REFERENCES

1. B.P. Gorman and H.U. Anderson, *J. Am. Ceram. Soc.* **85**, 981 (2002).
2. I. Kosacki, V. Petrovsky, and H.U. Anderson, *Appl. Phys. Lett.* **74**, 341 (1999).
3. V. Petrovsky, H.U. Anderson, and T. Petrovsky in *Nanocomposite Materials III*, edited by S. Komarneni, J.C. Parker, and H. Hahn, (Mater. Res. Soc. Symp. Proc. **581**, Warrendale, PA 2000) p. 553.
4. B.P. Gorman and H.U. Anderson, *J. Am. Ceram. Soc.* (2003, unpublished).
5. I. Kosacki, M. Shumsky, and H.U. Anderson, in *Ceramic Engineering and Science Proceedings 20*, edited by I. Ustundag and G. Fischman (The American Ceramic Society, Westerville, OH, 1999), p. 135.
6. D. Balzar, in *Defect and Microstructure Analysis by Diffraction*, edited by R.L. Snyder, J. Fiala, and H.J. Bunge (International Union of Crystallography, Oxford, U.K., 1999).
7. V. Petrovsky, B.P. Gorman, H.U. Anderson, and T. Petrovsky, in *Structure-Property Relationships of Oxide Surfaces and Interfaces*, edited by C.B. Carter, X. Pan, K. Sickafus, H.L. Tuller, and T.E. Wood, (Mater. Res. Soc. Symp. Proc. **654**, Warrendale, PA 2001) p. AA7.6.1.
8. B.P. Gorman and H.U. Anderson, *J. Am. Ceram. Soc.* **84**, 890 (2002).
9. D.W. Kingery, *Introduction to Ceramics*, 2nd ed. (John Wiley & Sons, New York, 1976).
10. A.W. Adamson, *Physical Chemistry of Surfaces*, 5th ed. (John Wiley & Sons, New York, 1990).
11. C.M. Flannery, P.V. Kelly, J.T. Beechinor, and G.M. Crean, *Appl. Phys. Lett.* **71**, 3767 (1997).
12. V. Petrovsky, B.P. Gorman, H.U. Anderson, and T. Petrovsky, *J. Appl. Phys.* **90**, 2517 (2001).
13. C. Murray, C. Flannery, I. Streiter, S.E. Schulz, M.R. Baklanov, K.P. Mogilnikov, C. Himcinschi, M. Friedrich, D.R.T. Zahn, and T. Gessner, *Microelectron. Eng.* **60**, 133 (2002).
14. B.C.H. Steele, *Solid State Ionics* **129**, 95 (2000).
15. H. Inaba and H. Tagawa, *Solid State Ionics* **83**, 1 (1996).
16. M. Mogensen, N.M. Sammes, and G.A. Tompsett, *Solid State Ionics* **129**, 63 (2000).
17. B. Djuricic and S. Pickering, *J. Eur. Ceram. Soc.* **19**, 1925 (1999).
18. J.R. Taylor, *An Introduction to Error Analysis*, 2nd ed. (University Science Books, Sausalito, CA, 1995).
19. O.S. Heavens, *Optical Properties of Thin Solid Films* (Dover, New York, 1995).
20. C.H. Peng and S.B. Desu, *J. Am. Ceram. Soc.* **77**, 929 (1994).